

Chapter 2

Mathematical Background

In this chapter we briefly review concepts from the theory of ill-posed problems, operator theory, linear algebra, estimation theory and sparsity. These concepts are used in the later chapters while doing convergence analysis of alternate minimization for blind image deconvolution and also for arriving at the appropriate regularizers for the image and the point spread function. We have stated theorems where needed without the proof.

We observed in Chap. 1 that under the assumption of a linear shift invariant blur, the image formation model consists of a convolution with a point spread function (PSF) and noise addition. The convolution was assumed to be circular, and the image being two dimensional, the convolution matrix is block circulant with circulant blocks. The convergence analysis in the later chapters proceed by using some properties of the BCCB matrices and these are briefly mentioned in Sect. 2.1. In the previous chapter we pointed out that the inherent difficulty of the blind deconvolution problem stems from the fact that it is an ill-posed problem. Understanding ill-posedness requires concepts from functional analysis. Section 2.2 on operator theory covers the concepts required for the analysis of ill-posed problems. In the next section we look at the different types of ill-posed problems and also methods of handling ill-posedness. We also show that blind deconvolution is a bilinear ill-posed problem. In addition to regularization based methods for blind deconvolution statistical estimation methods are also employed in solving the blind image deconvolution problem. The statistical estimation methods, maximum likelihood and maximum a posteriori probability are described next. Since the derivative domain and transform domain representation of images are sparse in nature, working in these domains gives the advantage of reduced computation owing to the sparse nature. We look into the feasibility of using sparsity based concepts for arriving at an appropriate regularizer. Basic concepts of sparsity are explained in Sect. 2.5. The chapter concludes with an overview of the optimization techniques used in this monograph.

2.1 Circulant Matrices

For analysis purpose we have taken the convolution in the image formation process to be circular throughout this monograph. It is seen from the image formation equation that under the assumption of circular convolution the PSF matrix obtained is block circulant with circulant blocks (BCCB). We briefly review a few relevant results on circulant matrices [31, 58] in this section.

Definition 2.1. A circulant matrix of order n is a square matrix where each row is obtained by circularly shifting the previous row by one place to the right.

An example is given below:

$$C = \begin{pmatrix} c_1 & c_2 & \cdots & c_n \\ c_n & c_1 & \cdots & c_{n-1} \\ \vdots & & & \\ c_2 & c_3 & \cdots & c_1 \end{pmatrix}.$$

The convolution matrix that arises in the case of 1-dimensional systems is circulant in nature. But for 2-dimensional signals the convolution matrix structure is not circulant but block circulant with circulant blocks which is defined next. A matrix C is block circulant if each row contains blocks which are circularly shifted. Let C_1, C_2, \dots, C_m be square matrices of order n . A block circulant matrix of order mn is of the form:

$$C = \begin{pmatrix} C_1 & C_2 & \cdots & C_m \\ C_m & C_1 & \cdots & C_{m-1} \\ \vdots & & & \\ C_2 & C_3 & \cdots & C_1 \end{pmatrix}.$$

A matrix in which each element is an order n block can exhibit circulant nature in an alternate manner – each of the blocks is circulant in nature. Such a matrix is called as a matrix with circulant blocks. It is of the form:

$$C = \begin{pmatrix} C_{11} & C_{12} & \cdots & C_{1m} \\ C_{21} & C_{22} & \cdots & C_{2m} \\ \vdots & & & \\ C_{m1} & C_{m2} & \cdots & C_{mm} \end{pmatrix},$$

where each C_{ij} is of order n and is circulant. Having defined a block circulant matrix and a matrix with circulant blocks, we now define a BCCB matrix.

Definition 2.2. A matrix is block circulant with circulant blocks (BCCB) if it is both block circulant and each block is circulant in nature.

Definition 2.3. A matrix C is unitary if

$$CC^{*T} = C^{*T}C = I,$$

i.e., the inverse of a unitary matrix is same as its conjugate transpose.

In the two definitions which follow, an $M \times N$ matrix

$$A = \begin{pmatrix} a(1, 1) & \cdots & a(1, N) \\ \vdots & & \vdots \\ a(M, 1) & \cdots & a(M, N) \end{pmatrix}$$

is represented as,

$$A = \{a(m, n)\} \quad 1 \leq m \leq M, 1 \leq n \leq N.$$

Definition 2.4. The discrete Fourier transform (DFT) matrix of order m is defined as

$$F_m = \left\{ \frac{1}{\sqrt{m}} W_m^{kn} \right\} \quad 0 \leq k, n \leq m-1,$$

where

$$W_m = e^{-j \frac{2\pi}{m}}.$$

Definition 2.5. Given two matrices A of size $M_1 \times M_2$ and B of size $N_1 \times N_2$, their Kronecker product is defined as

$$\begin{aligned} A \otimes B &= \{a(m, n)B\}, \\ &= \begin{pmatrix} a(1, 1)B & \cdots & a(1, M_2)B \\ \vdots & & \vdots \\ a(M_1, 1)B & \cdots & a(M_1, M_2)B \end{pmatrix}. \end{aligned}$$

Having defined the DFT matrix we come to an important theorem regarding BCCB matrices which is used extensively in this monograph.

Theorem 2.1. All BCCB matrices are diagonalizable by the unitary matrix $F_m \otimes F_n$.

F_m is the DFT matrix of order m and \otimes is the Kronecker product. If C is a BCCB matrix, then

$$C = (F_m \otimes F_n)^* A (F_m \otimes F_n), \quad (2.1)$$

where A is a diagonal matrix containing the eigenvalues of C which is same as the DFT of the first column of C . From Theorem 2.1 it follows that,

1. The set of BCCB matrices is closed under matrix addition and multiplication. This result is straightforward for matrix addition and for multiplication it follows since the DFT matrix is unitary.
2. Multiplication of BCCB matrices is commutative. This result again follows from the unitary nature of DFT matrix and from the fact that product of diagonal matrices commute.

2.2 Operator Theory

In this section we look at theorems from operator theory needed to understand the nature of ill-posed problems. The theorems are stated without proofs, as they can be found in any standard book on functional analysis [46, 74, 93].

Let \mathbf{X} and \mathbf{Y} be Hilbert spaces and \mathcal{A} a linear operator, $\mathcal{A} : \mathbf{X} \rightarrow \mathbf{Y}$. \mathcal{A} is bounded if there is an $\alpha > 0$ such that

$$\|\mathcal{A}(x)\| \leq \alpha \|x\|, \quad x \in \mathbf{X}. \quad (2.2)$$

The norm in Eq. (2.2) is the norm induced by the inner product in the Hilbert space, i.e., $\|x\| = \langle x, x \rangle^{1/2}$.

Theorem 2.2. \mathcal{A} is continuous if and only if \mathcal{A} is bounded.

Definition 2.6. Let \mathbf{H} be a Hilbert space and \mathcal{A} a bounded linear map. The unique bounded linear map \mathcal{A}^* such that

$$\langle \mathcal{A}x, y \rangle = \langle x, \mathcal{A}^*y \rangle$$

for all $x, y \in \mathbf{H}$ is called the adjoint of \mathcal{A} .

An operator is self adjoint if $\mathcal{A} = \mathcal{A}^*$.

Definition 2.7. Let \mathbf{H} be a Hilbert space. A linear operator \mathcal{A} is compact if for every bounded sequence (x_n) in \mathbf{H} , the image sequence $\mathcal{A}(x_n)$ has a convergent sub-sequence.

\mathcal{A} being compact implies that \mathcal{A} is bounded, the converse is not true in general. A compact operator \mathcal{A} cannot have a bounded (hence continuous) inverse unless its range has finite dimension. This is a result of the following two theorems [46, 93]:

Theorem 2.3. Let \mathbf{X} , \mathbf{Y} , and \mathbf{Z} be normed spaces and $\mathcal{K} : \mathbf{X} \rightarrow \mathbf{Y}$ and $\mathcal{L} : \mathbf{Y} \rightarrow \mathbf{Z}$ be bounded linear operators. Then the product $\mathcal{K}\mathcal{L} : \mathbf{X} \rightarrow \mathbf{Z}$ is compact if one of the operators is compact.

Theorem 2.4. *The identity operator $\mathcal{I} : \mathbf{X} \rightarrow \mathbf{X}$ is compact if and only if \mathbf{X} has a finite dimension.*

With $\mathbf{Y} = R(\mathcal{K})$ where $R(\mathcal{K})$ is the range of the operator \mathcal{K} and $\mathbf{Z} = \mathbf{X}$, \mathcal{L} becomes the inverse of \mathcal{K} . That is, $\mathcal{L}\mathcal{K} = \mathcal{K}^{-1}\mathcal{K} : \mathbf{X} \rightarrow \mathbf{X}$. Now $\mathcal{K}^{-1}\mathcal{K} = \mathcal{I}$. Since \mathcal{K} is compact, for infinite dimensional \mathbf{X} , \mathcal{K}^{-1} cannot be bounded. If it were, then it would imply from Theorem 2.3 that \mathcal{I} is compact for infinite dimensional \mathbf{X} which is not true. Hence the inverse operator is bounded (continuous) only when \mathbf{X} is finite dimensional.

The spectral theorem for compact self-adjoint operators is used for the analysis of linear ill-posed problems and we define it next. The spectrum of a bounded linear operator \mathcal{A} in Hilbert space \mathbf{H} is defined as [46,93]

$$\sigma(\mathcal{A}) = \{\lambda \in \mathbb{C} \mid \mathcal{A} - \lambda I \text{ has no bounded inverse}\}, \quad (2.3)$$

I is the identity operator on \mathbf{H} . If \mathcal{A} is self-adjoint then $\sigma(\mathcal{A})$ is a non-empty set of real numbers. For an operator \mathcal{A} , if $\mathcal{A}x = \lambda x$, $\lambda \in \mathbb{C}$, then λ is called as an eigenvalue and x an eigenvector associated with the eigenvalue λ . Every eigenvalue is an element of $\sigma(\mathcal{A})$. If \mathcal{A} is self-adjoint then the eigenvectors associated with distinct eigenvalues are orthogonal.

If the operator is compact in addition to being self-adjoint, each non-zero member of the spectrum is an eigenvalue of the operator. The spectrum contains the element zero if the space is infinite dimensional and the sequence of eigenvalues $\lambda_1, \lambda_2, \dots$ converges to zero for the infinite dimensional case. Also, for each non-zero eigenvalue (λ) of a compact self-adjoint operator, the associated eigenspace (which is the nullspace of the operator $\mathcal{A} - \lambda I$) is finite dimensional. Repeating each eigenvalue in the sequence of eigenvalues $\lambda_1, \lambda_2, \dots$ according to the dimension of its associated null-space, and listing out the eigenvectors, we get a sequence of orthonormal vectors. Using this the spectral theorem for a compact self-adjoint operator can be stated as [46,93],

Theorem 2.5. *Let $\mathcal{A} : \mathbf{H} \rightarrow \mathbf{H}$ be compact self-adjoint linear operator. Let $\lambda_1, \lambda_2, \dots$ be the eigenvalues (repeated according to the dimension of the associated eigenspace) and u_1, u_2, \dots be the associated eigenvectors. Then for any $x \in \mathbf{H}$*

$$\mathcal{A}(x) = \sum_n \lambda_n \langle x, u_n \rangle u_n.$$

The summation is finite or infinite depending on the number of eigenvalues. If A has finitely many eigenvalues then it is said to be of finite rank and corresponds to degenerate kernels for the space of square integrable functions.

2.3 Ill-posed Problems

In Chap. 1 we saw what makes the blind image deconvolution problem ill-posed. We repeat the definition of ill-posed problem for convenience of the reader. A problem is well-posed in the Hadamard sense [108] if the problem has a solution which is unique and if any small perturbation in the data leads to a similar change in the solution. This last condition indicates the stability of the solution to data perturbations. A problem which is not well-posed is an ill-posed one. In this section we see how to handle ill-posedness for the case of linear and non-linear ill-posed problems.

Let \mathbf{X} and \mathbf{Y} be Hilbert spaces and \mathcal{K} be a transformation from \mathbf{X} to \mathbf{Y} .

$$\mathcal{K} : \mathbf{X} \rightarrow \mathbf{Y}. \quad (2.4)$$

A problem of the form

$$\mathcal{K}(x) = y, \quad x \in \mathbf{X}, y \in \mathbf{Y}, \quad (2.5)$$

is called an inverse problem when the objective is to determine x , given y or its perturbed version y^δ

$$\|y - y^\delta\|^2 \leq \delta, \quad (2.6)$$

where δ can be thought of as the noise strength and is a small positive quantity. If the nature of \mathcal{K} is such that some information is lost in the forward process of formation of y from x , then the inverse problem of determining x from y becomes an ill-posed problem. Depending on whether \mathcal{K} is a linear or non-linear operator, the ill-posed problem is classified as linear or non-linear, respectively.

Assuming that the problem of existence and uniqueness of solution is appropriately handled, we will see how to handle the problem of stability of solution using the concept of regularization. We show in the next section that the ill-posedness of the blind deconvolution problem arises from the discretized image formation model and is because of the large condition number of the convolution matrix. With a large condition number the matrix is close to being singular and the inverse tends to amplify the noise. Regularizers provide a family of functions that approximate the inverse of a singular or close to singular operator [46, 50]. In other words, the ill-posed problem is replaced by a family of well-posed problems whose solutions are called as the regularized solutions that approximate the original solution.

In the following section we analyze the reason for the ill-posedness of blind deconvolution. The analysis is based on linear algebra. In the two sections which follow we show how regularization is used to obtain an approximate solution for the case of linear and non-linear ill-posed problems in an operator theory framework.

2.3.1 Blind Deconvolution as an Ill-posed Problem

In this section we see what makes the blind deconvolution problem inherently difficult to solve. Deconvolution when the PSF is known itself is a difficult problem to solve owing to the fact that it is an inverse problem. In most of the inverse problems the difficulty in solution arises due to the fact that some information is lost in the forward process, which makes inversion a difficult task. In order to get to the root of the problem, let us look at the image formation process which is an analog process. Under the assumptions of linearity and shift invariance, the image formation equation in the continuous domain is given by Eq. (1.6), which is repeated here for convenience.

$$y(u, v) = \int_{-\infty}^{\infty} \int_{-\infty}^{\infty} k(u - u_1, v - v_1) x(u_1, v_1) du_1 dv_1.$$

In image restoration $x(u, v)$ needs to be estimated from a noisy version of $y(u, v)$. This amounts to solving the integral equation in Eq. (1.6), which is a Fredholm integral equation of the first kind, the general form of which in one dimension is given by

$$\int_a^b \mathcal{K}(u, v) x(v) dv = y(u), \quad (2.7)$$

where $x(\cdot)$ is the unknown function, which is to be solved for, $\mathcal{K}(u, v)$ is the kernel and $y(u)$ is a known function.

It can be shown that an integral operator of the type in Eq. (2.7) is a compact operator by proving that it is a Hilbert-Schmidt operator [93].

Definition 2.8. Let H be a Hilbert space and $\mathcal{A} : X \rightarrow Y$ be a linear operator. \mathcal{A} is called a Hilbert-Schmidt operator if there is an orthonormal basis (v_n) of H such that

$$\sum_n \| \mathcal{A}(v_n) \|^2 < \infty.$$

If a bounded linear operator is Hilbert-Schmidt then it is compact [93]. It is a well known fact that [74, 93, 110],

Theorem 2.6. Let X and Y be normed spaces and let $\mathcal{A} : X \rightarrow Y$ be a compact linear operator. \mathcal{A} cannot have a bounded inverse if X is infinite dimensional.

It may be noted that Theorem 2.6 follows from Theorems 2.3 and 2.4. From Theorem 2.6 it is inferred that the inverse operator of Eq. (2.7) is not continuous. Since Eq. (1.6) is of the form Eq. (2.7), the inverse operator in this case is also discontinuous. This leads to instability of the solution making the problem an ill-posed one. An alternate way to see the instability in solution of the integral

equation in Eq. (2.7) is by making use of the Reimann-Lebesgue lemma [124]. From Riemann-Lebesgue lemma, for any integrable kernel, the integral

$$\int_a^b \mathcal{K}(u, v) \sin(mv) dv \rightarrow 0 \text{ as } m \rightarrow \infty,$$

and the integral tends to zero faster for smooth kernels than for sharp ones. If $x(v)$ is a solution to Eq. (1.6), then

$$\int_a^b \mathcal{K}(u, v)(x(v) + \sin(mv))dv = y(u) + \int_a^b \mathcal{K}(u, v) \sin(mv)dv. \quad (2.8)$$

As $m \rightarrow \infty$, the perturbation in y is infinitesimal, whereas there is a finite change for x , indicating instability – the solution is sensitive to high frequency perturbations. Since in image deconvolution we work in the finite dimensional discrete domain, the problem of discontinuous inverse does not exist since in this case a compact linear operator always has a continuous inverse. Yet, since the finite dimensional case is obtained by discretizing an ill-posed problem, the effect of ill-posedness of the continuous operator on the behavior of the discrete problem needs to be explored.

For the image formation model in Eq. (1.5), discretization gives an expression of the form Eq. (1.9) with the noise term being zero. Here K is the finite dimensional approximation of the kernel \mathcal{K} . It has been noted [9, 73, 124] that, instability in solution of the continuous domain formulation Eq. (1.5) gets reflected in the condition number of its finite dimensional approximation. It is observed that the condition number depends on the quality of the discretization. Finer the quality of discretization, higher is the condition number aggravating the stability issues while doing the image restoration. An explanation for this behavior is given in [128]. Using the fact that the convolution matrix K is the discretized version of the kernel \mathcal{K} and using Taylor's theorem, it was shown in [128] that, any row of K is approximately a linear combination of the adjacent rows leading to a nearly singular matrix. It is also shown that, finer the discretization, better the approximation, which makes K more ill-conditioned.

It may be noted that though the continuous domain formulation is ill-posed due to stability issues, the equivalent discrete domain problem is not ill-posed strictly in the sense of the third condition for ill-posedness. If the discretization is coarse, then the condition number is small and a solution can still be obtained, but as the fineness of the discretization increases, the behavior of the discrete problem approximates the unstable behavior of the continuous equivalent, in the sense that it becomes sensitive to high frequency perturbations. The effect of the condition number on the usability of the estimated solution is analyzed next.

The convolution matrix K being BCCB, is diagonalized by the DFT matrix. i.e.

$$K = F^* \mathcal{D} F, \quad (2.9)$$

where F is the 2D DFT matrix, F^* its conjugate transpose which is same as the inverse in this case (i.e. $F^{-1} = F^*$) since the DFT matrix is unitary. \mathcal{D} is a diagonal matrix with diagonal entries corresponding to the DFT of the first column of K , which is also same as the eigenvalues of K . Let the columns of F^* be represented by v_k , $k = 0, 1, \dots, N$, then Eq. (2.9) becomes

$$K = \sum_{k=1}^N \lambda_k v_k v_k^*, \quad (2.10)$$

where λ_k are the eigenvalues of K . v_k^* is the conjugate transpose of v_k . For noisy observations, from Eq. (1.9)

$$\begin{aligned} \underline{y} &= K \underline{x} + \underline{n}, \\ &= \sum_{k=1}^N \lambda_k v_k v_k^* \underline{x} + \underline{n}. \end{aligned} \quad (2.11)$$

where Eq. (2.10) is used for K . Since the PSF is usually a low pass filter, the high frequency spectral content is low which corresponds to small eigenvalues. For very low eigenvalues it may be seen from Eq. (2.11) that the noise dominates over the signal and for an image this signal component corresponds to the edges. Provided K^{-1} exists, a possible estimate for the image (\hat{x}) is

$$\begin{aligned} \hat{\underline{x}} &= K^{-1} \underline{y}, \\ &= \underline{x} + K^{-1} \underline{n}. \end{aligned} \quad (2.12)$$

From Eqs. (2.9) and (2.10)

$$\begin{aligned} K^{-1} &= F^* \mathcal{D}^{-1} F, \\ &= \sum_{k=1}^N \frac{v_k v_k^*}{\lambda_k}. \end{aligned} \quad (2.13)$$

Using Eq. (2.13), in Eq. (2.12) we get

$$\hat{\underline{x}} = \underline{x} + \sum_{k=1}^N \frac{v_k (v_k^* \underline{n})}{\lambda_k}. \quad (2.14)$$

From Eq. (2.14) we see that even though the original image is extracted by the inverse, there is a noise component added to this. For eigenvalues close to zero, the noise amplification is very high making the estimate unusable. The ill-posed nature is evident here, since a small change in the data leads to a large variation in the estimated image. Let the error in the data be upper bounded by δ , i.e.

$$\| \underline{y}^\delta - \underline{y} \| \leq \delta, \quad (2.15)$$

where \underline{y}^δ is the perturbed observation. From Eq. (2.14), the corresponding error in the estimate is

$$\|\hat{\underline{x}} - \underline{x}\|^2 = \sum_{k=1}^N \frac{|v_k^*(\underline{y}^\delta - \underline{y})|^2}{\lambda_k^2}. \quad (2.16)$$

Let the eigenvalues be arranged such that $0 \leq |\lambda_1| \leq \dots \leq |\lambda_N|$. It can be seen that

$$\text{If } \underline{y}^\delta - \underline{y} = \delta v_1, \text{ then } \|\hat{\underline{x}} - \underline{x}\| = \delta/|\lambda_1|$$

$$\text{If } \underline{y}^\delta - \underline{y} = \delta v_N, \text{ then } \|\hat{\underline{x}} - \underline{x}\| = \delta/|\lambda_N|.$$

This implies that for low frequencies (large eigenvalues), the effect of noise on the reconstructed signal is very less, whereas for high frequencies the signal is severely corrupted by noise. This is characteristic of ill-posed problems – the same amount of noise in different frequency bands is treated differently. It may also be noted that λ_1 , the smallest eigenvalue determines the condition number of a matrix which is defined as

$$\kappa = \frac{|\lambda_N|}{|\lambda_1|}. \quad (2.17)$$

As λ_1 tends to zero, the matrix becomes more ill-conditioned leading to instability of the solution. These facts can also be inferred from a frequency domain analysis. A complete frequency domain analysis of the problem can be found in [9]. Since the results w.r.t. stability are same, we provide only a summary of the existence and uniqueness conditions here. The frequency domain equivalent of Eq. (1.6) in the presence of additive noise is

$$\mathcal{Y}(\Omega) = \mathcal{K}(\Omega)\mathcal{X}(\Omega) + \mathcal{N}(\Omega), \quad (2.18)$$

where \mathcal{Y} , \mathcal{X} , and \mathcal{K} denote the Fourier transform for the continuous case, and $\Omega = [\Omega_x, \Omega_y]$. Since the system is linear, the condition for uniqueness of solution is

$$\mathcal{K}(\Omega)\mathcal{X}(\Omega) = 0, \quad (2.19)$$

only when $\mathcal{X}(\Omega) = 0$. If the system is band limited, this is not true and a unique solution does not exist. Assuming that $\mathcal{K}(\Omega)$ has the entire frequency axis as its support, we can look at the condition for existence of solution. As in Eq. (2.14) in spatial domain, a estimate in the frequency domain is obtained as

$$\hat{\mathcal{X}}(\Omega) = \mathcal{X}(\Omega) + \frac{\mathcal{N}(\Omega)}{\mathcal{K}(\Omega)}. \quad (2.20)$$

Now, the existence of solution depends on the existence of inverse Fourier transform of Eq. (2.20). For the case of motion blur, the frequency response of the imaging system is zero for some frequencies, whereas the noise spectrum is assumed to be uniform through the spectrum (under the assumption of white noise). This leads to singularities at the zeros of the PSF and the inverse of $\hat{\mathcal{X}}(\Omega)$ may not exist. Even if $\mathcal{H}(\Omega)$ is not zero, it tends to zero as $\Omega \rightarrow \infty$, but the ratio $\frac{\mathcal{N}(\Omega)}{\mathcal{H}(\Omega)}$ may not tend to zero. Hence the existence of the inverse Fourier transform depends on the behavior of this ratio, and the condition for existence of inverse can be expressed as,

$$\int \left| \frac{\mathcal{N}(\Omega)}{\mathcal{H}(\Omega)} \right| d\Omega < \infty. \quad (2.21)$$

In general Eq. (2.21) does not hold for noisy images, and hence the solution exists only for noise free images. The uniqueness and existence in the discrete case can also be determined on similar lines. The above analysis is for the case where the PSF is known. In the case of blind deconvolution the problem is more complicated due to the fact that the PSF is not known. This makes the problem highly nonlinear, and there exists an infinite number of solutions of the form $(a\hat{x}, \hat{k}/a)$, where $a \in \mathbf{R}^+$. Though the solution space can be reduced by using the constraints on PSF and using known properties of the image, the problem of stability still persists. Next we see the two different classes of ill-posed problems namely the linear and non-linear ill-posed problems.

2.3.2 Linear Ill-posed Problems

For the linear case, \mathcal{H} in Eq. (2.4) is a bounded linear operator from \mathbf{X} to \mathbf{Y} . In the continuous case, the operator is denoted by \mathcal{H} and its discretized version which is a matrix is written as K . Due to the ill-conditioned nature of the problem we look for a vector which is ‘near’ to the solution instead of an exact solution. The best approximate solution \hat{x} for $Kx = y$ is taken as the minimum-norm least squares solution [33] i.e.,

$$\|\hat{x}\| = \inf \{\|Kx - y\| \mid x \in X\}. \quad (2.22)$$

It is proved in [33] that there exists a unique best approximate solution given by

$$\hat{x} = K^\dagger y, \quad (2.23)$$

where K^\dagger is the Moore-Penrose generalized inverse. Also $x \in X$ is a least squares solution if and only if

$$K^* Kx = K^* y, \quad (2.24)$$

i.e., $K^\dagger = (K^*K)^{-1}K^*$, where K^* is the adjoint of K and for real valued K the adjoint K^* reduces to the transpose K^T .

As mentioned in the Sect. 2.2, if K is compact and the range of K is infinite dimensional then K^\dagger is unbounded and hence discontinuous leading to ill-posedness. From the spectral theorem, for a compact self-adjoint linear operator there exists a singular system defined as $(\sigma_n; v_n, u_n)$ [46, 93], where σ_n^2 are the non-zero eigenvalues of the operator K^*K , written in decreasing order, $\{v_n\}$ are the corresponding orthonormal system of eigenvectors of K^*K , and $\{u_n\}$ are the orthonormal system of eigenvectors for KK^* . The condition for existence of a best approximate solution is given by Picard criterion [33], which says that such a solution exists if the Fourier coefficients $(\langle y, u_n \rangle)$ decay fast enough relative to the singular values σ_n . For compact linear operators whose range is infinite dimensional the eigenvalues tend to zero as $n \rightarrow \infty$ which leads to noise amplification as we saw in the previous section. Faster the eigenvalues decay, stronger is the error amplification. Using this fact, ill-posedness can be quantified as mild or severe depending on polynomial or exponential decay, respectively, of the eigenvalues.

Unboundedness of K^\dagger leads to ill-posedness since the inverse is not continuous in this case and this creates problem when the data is noisy. Let y^δ be the noisy observation with

$$\|y^\delta - y\| \leq \delta, \quad (2.25)$$

where δ is the noise variation. Owing to the discontinuity of K^\dagger , $K^\dagger y^\delta$ is not a good approximation to $K^\dagger y$. This necessitates finding an approximation to the best approximate solution $\hat{x} = K^\dagger y$ when the data is noisy. To handle instability it is required to find a continuous function that approximates K^\dagger and gives a solution x_α^δ which converges to \hat{x} when $\delta \rightarrow 0$ with a proper choice of α . This is achieved by replacing K^\dagger by a family $\{R_\alpha\}$ of continuous operators referred to as regularization operators, which depend on the parameter α (the regularization factor). With this

$$x_\alpha^\delta = R_\alpha y^\delta, \quad x_\alpha^\delta \rightarrow x^\dagger, \text{ when } \delta \rightarrow 0. \quad (2.26)$$

A family of operators $\{R_\alpha\}$ exists since there exists a collection of equations, $Kx = y^\delta$, corresponding to different values of δ . Fixing a value for α depends on a specific equation due to its dependency on δ . In the discrete case, the requirement of a continuous inverse is equivalent to the condition number of the matrix equivalent of K^\dagger being small. We describe two types of regularizers below – the Tikhonov regularizer and the bounded variation regularization. Since we focus only on estimation of the discrete image, these regularizers are explained in the discrete domain.

2.3.2.1 Tikhonov Regularization

We observed in Sect. 2.3.1 that in the presence of noise, oscillations appear in the solution of Fredholm integral equation. Tikhonov [50, 122, 157] proposed usage of an additional term to smooth out such oscillations. A spectral theory based development [33, 46] of the Tikhonov regularizer is given below.

Given the singular system $(\sigma_n; v_n, u_n)$ for the compact linear operator K , $K^\dagger y$ can be written as

$$K^\dagger y = \sum_{n=1}^{\infty} \frac{\langle K^* y, v_n \rangle}{\sigma_n^2} v_n. \quad (2.27)$$

To regularize K^\dagger the amplification factors $\frac{1}{\sigma_n^2}$ is replaced by a modified version $U(\alpha, \sigma_n^2)$ [33]. This gives

$$x_\alpha^\delta = \sum_{n=1}^{\infty} U(\alpha, \sigma_n^2) \langle K^* y^\delta, v_n \rangle v_n. \quad (2.28)$$

The choice of $U(\alpha, \sigma_n^2)$

$$U(\alpha, \sigma_n^2) = \frac{1}{\alpha + \sigma_n^2}, \quad (2.29)$$

leads to the Tikhonov regularizer. This, along with $Kv_n = \sigma_n u_n$ gives

$$x_\alpha^\delta = \sum_{n=1}^{\infty} \frac{\sigma_n}{\alpha + \sigma_n^2} \langle y^\delta, u_n \rangle v_n. \quad (2.30)$$

In terms of the operator K , x_α^δ given in Eq. (2.30) can be written as

$$x_\alpha^\delta = (\alpha I + K^* K)^{-1} K^* y^\delta. \quad (2.31)$$

This is the solution obtained by minimizing the cost

$$C_\alpha^\delta(x) = \|Kx - y^\delta\|^2 + \alpha \|x\|^2. \quad (2.32)$$

The presence of $\alpha \|x\|^2$ stabilizes the solution. It penalizes solutions which are of large amplitude, possibly due to error amplification. Penalty terms of a more general form such as $\|\mathcal{L}x\|^2$ could be used where \mathcal{L} is usually a derivative based operator that enforces smoothness. With $\|\mathcal{L}x\|^2$ as the regularizer the estimate becomes

$$C_\alpha^\delta(x) = (\alpha \mathcal{L}^* \mathcal{L} + K^* K)^{-1} K^* y^\delta. \quad (2.33)$$

To see the effect of the regularization parameter α , we split Eq. (2.30) by using the image formation model $y^\delta = Kx + n$, where n is AWGN. This model is same as in Eq. (1.9), only the notation is changed.

$$x_\alpha^\delta = \sum_{n=1}^{\infty} \frac{\sigma_n^2}{\alpha + \sigma_n^2} \langle x, v_n \rangle v_n + \sum_{n=1}^{\infty} \frac{\sigma_n}{\alpha + \sigma_n^2} \langle n, u_n \rangle v_n. \quad (2.34)$$

It is seen from Eq. (2.34) that for small values of α the first term is approximately x and the second term leads to noise amplification since the denominator is dominated by σ_n^2 . This amounts to having no regularization. If α is large, the effect of noise amplification is less, but the solution deviates from x . Hence the regularization factor should be selected such that there is a balance between stability and accuracy.

The problem with using a regularization of the form Eq. (2.33) in image restoration is that the solution is excessively smooth since the edges in the image are penalized by the regularizer. Since \mathcal{L} is a derivative operator its eigenvalues increases as $n \rightarrow \infty$. With $\mathcal{L}x$ as the regularizer, the solution becomes

$$x_\alpha^\delta = \sum_{n=1}^{\infty} \frac{\sigma_n^2}{\alpha \gamma_n^2 + \sigma_n^2} \langle x, v_n \rangle v_n + \sum_{n=1}^{\infty} \frac{\sigma_n}{\alpha \gamma_n^2 + \sigma_n^2} \langle n, u_n \rangle v_n, \quad (2.35)$$

where γ_n is the eigenvalue of the differential operator γ_n . Differential operators are unbounded and in the case where they have a compact self-adjoint inverse, the eigenvalues of the operator is the reciprocal of the eigenvalues of the inverse operator. As was mentioned earlier the eigenvalues of a compact self-adjoint operator tends to zero as $n \rightarrow \infty$, when there are infinite of them. Assuming that \mathcal{L} has a compact self-adjoint inverse, γ_n increases as $n \rightarrow \infty$. Since γ_n increases and σ_n decreases with n it can be seen from Eq. (2.35) that the amount of regularization depends on n which corresponds to frequency in the signal processing perspective. For small frequencies since γ_n is close to zero, the signal is reproduced faithfully. The noise component gets attenuated more as frequency increases since the denominator of the second term increases with n . With increase in n it is also seen that the first term gets attenuated more leading to loss of high frequency information in x which corresponds to edge information in image, leading to smoothing of the image. It may be noted that the regularizer corresponds to a high-pass filter and the blur term to a low-pass filter in a signal processing perspective. This aspect is further discussed in Chap. 3. In order to avoid smoothing of the solution we need to use a regularizer which permits edges in the solution. Total variation which is one such regularizer, is described next.

2.3.2.2 Bounded Variation Regularization

A function of bounded variation is one with a finite total variation. For a continuous function $f(u)$, the total variation is defined as [137]

$$TV(f(u)) = \int_a^b |f'(u)| du. \quad (2.36)$$

This measures the amount by which the function changes along the ordinate as the value of the independent variable changes from a to b . For a differentiable function of two variables $f(u, v)$, total variation becomes

$$TV(f(u, v)) = \int_a^b \int_c^d |\text{grad } f(u, v)| du dv, \quad (2.37)$$

where $\text{grad } f$ is the gradient of the function f and $|\text{grad } f(u, v)|$, the magnitude of the gradient is $\sqrt{f_u^2 + f_v^2}$, with f_u, f_v being the first order horizontal and vertical derivatives, respectively. The isotropic discrete total variation function for an image [8, 15] is defined as

$$TV(x) = \sum_j \sqrt{\Delta^h(x_j)^2 + \Delta^v(x_j)^2}, \quad (2.38)$$

where Δ^h and Δ^v are the first-order horizontal and vertical differences, respectively, and j is the pixel index. It can be seen as the sum of magnitude of the gradient at each pixel location. $TV(x)$ can be seen as a mixed norm, since at each pixel location an ℓ_2 norm (of the gradient at that point) is taken, followed by summation of the positive square root values which amounts to an ℓ_1 norm. Replacing the stabilizing term of Eq. (2.32) with Eq. (2.38), leads to total variation regularization which permits solutions that can capture sharp features in the original image.

Unlike the Tikhonov regularizer, here the regularization term is non-quadratic. In order to make analysis feasible we approximate the TV function by its quadratic upper bound [40]. Since Eq. (2.38) is the sum of square root of a quadratic function, an obvious way to upper bound $TV(x)$ is by upper bounding the square root function [40]. This is illustrated in Fig. 2.1. From Fig. 2.1

$$\sqrt{x_2} \leq \sqrt{x_1} + \frac{1}{2\sqrt{x_1}}(x_2 - x_1), \quad x_2 \geq x_1, x_1 > 0. \quad (2.39)$$

where $\frac{1}{2\sqrt{x_1}}$ is the slope of \sqrt{x} at the point x_1 . Using Eq. (2.39) in Eq. (2.38)

$$\begin{aligned} TV(x) &\leq Q_{TV}(x, x^{(i)}), \\ &\triangleq \sum_j \frac{1}{2} \frac{(\Delta^h x_j)^2 + (\Delta^v x_j)^2}{\sqrt{(\Delta^h x_j^{(i)})^2 + (\Delta^v x_j^{(i)})^2}} + B(x^{(i)}), \end{aligned} \quad (2.40)$$

where i is the iteration number, $x^{(i)}$ is the point w.r.t. which the value of TV function at x is approximated. $B(x^{(i)})$ is a constant term, independent of the

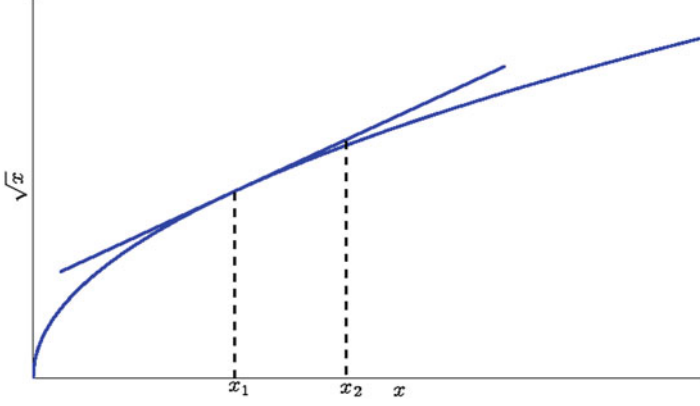


Fig. 2.1 Illustration of upper bounding the square root function

variable x . The right hand side of the inequality Eq. (2.40) is a quadratic function of the first order difference of image pixel values. The first term of Eq. (2.40) can be written as a matrix vector product by defining a difference operation matrix $D = [(D^h)^T (D^v)^T]^T$. D^h and D^v denote matrices such that $D^h \underline{x}$ and $D^v \underline{x}$ are the vectors of all horizontal and vertical first-order differences of the vector x , respectively (\underline{x} is the vector obtained by row ordering the matrix x). Periodic boundary condition is used for x while computing the first-order difference. Using the operator D , Eq. (2.40) becomes

$$Q_{TV}(\underline{x}, \underline{x}^{(i)}) = \underline{x}^T D^T \Lambda^{(i)} D \underline{x} + B(\underline{x}^{(i)}), \quad (2.41)$$

where $\Lambda^{(i)}$ takes care of the denominator of the first term in RHS of Eq. (2.40) and is defined as

$$\Lambda^{(i)} = \text{diag}(W^{(i)}, W^{(i)}), \quad (2.42)$$

where $\text{diag}(L)$ refers to a diagonal matrix with elements of vector L as the diagonal and $W^{(i)}$ is a vector whose j th element is

$$w_j^{(i)} = \left(2\sqrt{(\Delta^h x_j^{(i)})^2 + (\Delta^v x_j^{(i)})^2} \right)^{-1}. \quad (2.43)$$

In all our formulations with TV as regularizer we use the upper bounded function in Eq. (2.41) as the regularizer.

2.3.3 Non-linear Ill-posed Problems

An ill-posed problem is classified as non-linear, when \mathcal{K} in Eq. (2.4) is a non-linear operator. Since spectral analysis is infeasible in this case, finding a regularizer

and regularization factor is not as straight forward as in the linear ill-posed case. Tikhonov regularization and iterative methods [33,50] are two widely used methods for solving non-linear ill-posed problems. With \mathcal{K} non-linear, Eq. (2.32) can be rewritten as

$$C_{\alpha}^{\delta}(x) = \| \mathcal{K}(x) - y^{\delta} \|^2 + \alpha \| x \|^2. \quad (2.44)$$

and it can be seen that uniqueness of the solution is not guaranteed in this case. With \mathcal{K} non-linear, Eq. (2.44) is not convex and may have local minima in which a descent method could get stuck. Also determination of a proper regularization factor is difficult in this case. Owing to these difficulties iterative regularization methods are preferred for the non-linear case.

In iterative methods x is estimated starting from an initial guess x_0 as

$$x_{i+1} = x_i + \mathcal{K}'(x_i)^{-1}(y - \mathcal{K}(x_i)), \quad (2.45)$$

where \mathcal{K}' is the Frechet derivative of \mathcal{K} [50]. This is similar to the Newton's method, with the difference that the derivative of the function is replaced by the Frechet derivative which is defined below [119,126].

Definition 2.9. Let \mathbf{X} and \mathbf{Y} be two normed linear spaces. A mapping $\mathcal{F} : \mathbf{X} \rightarrow \mathbf{Y}$ is said to be Frechet differentiable at $x \in \mathbf{X}$ if there exists a bounded linear mapping $\mathcal{A} : \mathbf{X} \rightarrow \mathbf{Y}$ such that

$$\lim_{h \rightarrow 0} \frac{\| \mathcal{F}(x+h) - \mathcal{F}(x) - \mathcal{A}h \|_{\mathbf{Y}}}{\| h \|_{\mathbf{X}}} = 0.$$

The linear operator \mathcal{A} is called the Frechet derivative of \mathcal{F} at x .

Frechet derivative defines the derivative of an operator and is given by the bounded linear operator \mathcal{A} . This concept is similar to that of the derivative of functions, wherein the derivative represents the slope of the tangent at the point and is the best linear approximation in the neighborhood of the point at which the derivative is taken. For ill-posed problems the inverse of \mathcal{K}' is usually unbounded because of which one has to solve a linear ill-posed problem in each step of the iteration by using a regularizer. Hence an iterative method of the form Eq. (2.45) is inappropriate. An alternative is to use Landweber iteration [50] which is a steepest descent method leading to an update equation of the form

$$x_{i+1} = x_i + \mathcal{K}'(x_i)^*(y - \mathcal{K}(x_i)), \quad (2.46)$$

where $\mathcal{K}'(x_i)^*$ is the adjoint of the Frechet derivative. Here the negative gradient of the functional $\frac{1}{2} \| y - \mathcal{K} \|^2$ (second term in Eq. (2.46)) decides the update direction for the current iteration. In Eqs. (2.45) and (2.46), i indicates the iteration.

Due to the ill-posed nature of the problem, the iterations must be stopped at an appropriate time or stopping index i_* . An appropriate value of i_* can be chosen as a function of the perturbation in the data δ . The index i_* can be determined using

$$\|y^\delta - F(x_{i_*}^\delta)\| \leq \tau\delta < \|y^\delta - F(x_i^\delta)\|, \quad 0 \leq i < i_*, \quad (2.47)$$

for some sufficiently large $\tau > 0$. This condition ensures that the error is less than $\tau\delta$ when the number of iterations becomes i_* .

2.3.4 Bilinear Ill-posed Problems

In this section we show that the blind deconvolution problem is a bilinear ill-posed problem. Equation (2.5) is similar to the image formation equation (1.9) with \mathcal{K} being the convolution matrix K . In the case of blind deconvolution, the operator K which is the convolution matrix corresponding to the point spread function is not known which may make the blind deconvolution problem look like a non-linear ill-posed problem, since both K and \underline{x} are unknowns. Considering the image and the PSF as unknowns, the image formation process can be seen as mapping of the form

$$\mathcal{G} : \mathbf{X} \times \mathbf{K} \rightarrow \mathbf{Y}, \quad (2.48)$$

where \mathbf{K} is the Hilbert space consisting of the PSFs. The image formed \underline{y} can be written in terms of the mapping as

$$\begin{aligned} \underline{y} &= \mathcal{G}(\underline{x}, K), \\ &= K\underline{x}, \end{aligned} \quad (2.49)$$

in the no-noise case. Keeping one of the variables, say K , constant it is seen from Eq. (2.50) that the operator \mathcal{G} is linear in the other variable \underline{x}

$$\begin{aligned} \mathcal{G}(\alpha_1 \underline{x}_1 + \alpha_2 \underline{x}_2, K) &= K(\alpha_1 \underline{x}_1 + \alpha_2 \underline{x}_2) \\ &= \alpha_1 K\underline{x}_1 + \alpha_2 K\underline{x}_2 \\ &= \alpha_1 \mathcal{G}(\underline{x}_1, K) + \alpha_2 \mathcal{G}(\underline{x}_2, K), \end{aligned} \quad (2.50)$$

where α_1 and α_2 are constants. Similarly by fixing \underline{x} and using the constants β_1 and β_2 , it is seen that the operator is linear in the PSF variable K

$$\mathcal{G}(\underline{x}, \beta_1 K_1 + \beta_2 K_2) = \beta_1 \mathcal{G}(\underline{x}, K_1) + \beta_2 \mathcal{G}(\underline{x}, K_2). \quad (2.51)$$

From Eqs. (2.50) and (2.51) we conclude that the blind deconvolution process is a bilinear ill-posed problem. Since keeping one of the variables fixed reduces the

problem to a linear ill-posed one, solving the blind deconvolution problem amounts to solving two linear ill-posed problems that are coupled. Solution for problems of this type is pursued in Sect. 2.6.

2.4 Estimation of Random Field

In the above sections we considered image to be a deterministic signal and used regularization methods to handle the ill-posedness of blind deconvolution. An alternative to this is to use statistical estimation methods. Here the image is considered to be a stochastic signal, with each pixel represented as a random variable. Such a statistical representation of an image is called a random field [58]. There exists a rich structure in natural images and, in general, the neighboring pixels have similar values except at the edges. This structure is often captured by a Markov random field (MRF) [20, 58]. Given a pixel at location (i, j) , let its limited neighborhood be represented by $N(i, j)$. Let X_{ij} be the random variable representing the pixel value at (i, j) . A given random field shows the Markov property if

$$P(X_{ij} = x_{ij} | X_{kl} = x_{kl}, \forall (k, l) \neq (i, j)) = P(X_{ij} = x_{ij} | X_{kl} = x_{kl}, \forall (k, l) \in N(i, j)), \quad (2.52)$$

i.e., the value of a pixel depends only upon the value of its neighboring pixels. With Markov property one can only get the conditional distribution of the random field, whereas one needs the joint distribution of the pixels in the random field to serve as the prior. The joint distribution can be obtained using the Hammersley-Clifford theorem [10] which establishes a one to one correspondence between an MRF and a Gibbs distribution. Before proceeding to the theorem we would define the Gibbs distribution for which one needs to define a clique. Given a neighborhood $N(i, j)$ for a pixel, a clique is either a single pixel location or a pair such that if (i, j) and (k, l) belong to a clique (c) , then $(k, l) \in N(i, j)$. We do not discuss higher order cliques here. Let the collection of all cliques c be denoted by C .

Definition 2.10. A random field with a neighborhood structure $N(i, j)$ defined on it is a Gibbs random field *iff* its joint distribution is of the form

$$P(X = x) = \frac{1}{Z} \exp(-U(x)), \quad (2.53)$$

where $U(x)$ is the energy function associated with all the cliques and is defined as

$$U(x) = \sum_{c \in C} V_c(x),$$

where $V_c(x)$ is the clique potential associated with the clique c and Z is the partition function given by

$$Z = \sum_x U(x).$$

Here the summation is carried out over the entire configuration space of the variable x .

We now state the Hammersley-Clifford theorem without proof, the proof can be found in [10].

Theorem 2.7. *Let $N(i, j)$ be a neighborhood system defined on a random field. The random field is a Markov random field w.r.t. $N(i, j)$ iff its joint distribution is a Gibbs distribution with cliques associated with $N(i, j)$.*

Using this theorem one can obtain a joint distribution for a natural image which can be used as a prior for the image.

In the image formation model in Eq. (1.9) we assumed the noise to be white Gaussian leading to a random vector \underline{n} consisting of Gaussian distributed random variables which are independent with mean zero and variance same as the noise variance (σ_n^2). Hence given the original image \underline{x} and the PSF \underline{k} , \underline{y} is a random vector which also consists of independent Gaussian random variables with means $K\underline{x}$ and variance σ_n^2 . With this, the likelihood of \underline{y} can be written as

$$f(\underline{y}|\underline{x}, \underline{k}) \propto \exp\left(-\frac{\|\underline{y} - K\underline{x}\|^2}{2\sigma_n^2}\right). \quad (2.54)$$

The a posteriori probability for the image and the PSF is

$$f(\underline{x}, \underline{k}|\underline{y}) = \frac{f(\underline{y}|\underline{x}, \underline{k})f(\underline{x})f(\underline{k})}{f(\underline{y})}, \quad (2.55)$$

where the density corresponding to a variable is to be understood from the argument (i.e. $f_x(x)$ is written as $f(x)$). We have assumed that the image and the PSF are independent random vectors. Here $f(x)$ and $f(k)$ are the priors of the image and the PSF, respectively. Since the image and the PSF both can be seen as random fields, following the discussion at the beginning of this section, both can be seen as Markov random fields and a prior can be assigned using the Hammersley-Clifford theorem. Usually this gives rise to the quadratic prior which enforces smoothness in the solution.

In maximum likelihood (ML) estimation, \underline{x} , and \underline{k} which maximize the likelihood need to be estimated. Instead of maximizing the likelihood as given in Eq. (2.54), its negative logarithm is minimized.

$$(\hat{\underline{x}}, \hat{\underline{k}}) = \arg \min_{\underline{x}, \underline{k}} \lambda \|\underline{y} - K\underline{x}\|^2, \quad (2.56)$$

where λ replaces the unknown noise variance. Similarly in maximum a posteriori probability (MAP) estimate, the negative logarithm of a posteriori probability is minimized to estimate the image and the PSF which maximize the a posteriori probability. The MAP estimate is given by

$$(\hat{\underline{x}}, \hat{\underline{k}}) = \arg \min_{\underline{x}, \underline{k}} \| \underline{y} - K \underline{x} \|^2 - \lambda_x \log f(\underline{x}) - \lambda_k \log f(\underline{k}), \quad (2.57)$$

where λ_x and λ_k replace the noise variance. Since both the image and the PSF are unknowns, ML cannot be used directly for estimating the unknowns. But ML is used in blind deconvolution for estimating model parameters in the case where the image and PSF are modeled using ARMA (auto regressive moving average) model; this is given in more detail in Chap. 3. Since in MAP estimation additional information in the form of prior is present it is more suited for blind deconvolution; this is discussed further in Chap. 4. It may also be noted that MAP estimation is like the regularized estimation with the priors acting as regularizers. One way of modeling the blur prior is using parametric models like the linear motion blur, out-of-focus blur and the atmospheric turbulence blur, the details of which were given in Chap. 1. Another way of assigning prior to image and blur is by making use of the structure present in image/blur to restrict the solution space to that of the most probable solutions. This amounts to the regularization method used to convert an ill-posed problem to a well-posed one. Since natural images are smooth/piecewise smooth/textured, this information can be captured in stochastic models and be used as the prior [123]. The priors are specified by taking into consideration the probabilistic relations between neighboring pixels in the image or the PSF as discussed.

2.5 Sparsity Inducing Norms

Sparsity is a suitable concept which can be used for finding appropriate regularizers for an image since images are often sparse in the derivative domain and in the transform domain. In this section we introduce the concept of sparsity and also look at sparsity inducing norms that can be used as potential regularizers.

A signal or vector can be termed as sparse if most of the energy of the signal is concentrated on a few samples and the remaining samples are zero. It is a well known fact that the ℓ_1 norm induces sparsity i.e., using ℓ_1 norm as a regularizer while solving problems of the form $Ax = b$ leads to solutions which have more number of zeros. Reviewing the literature [12,22,32,156] it is seen that this tendency of ℓ_1 norm is accepted as a heuristic and there exists only graphical ways of explaining this behavior. For purpose of completeness we describe the graphical reasoning for sparsity inducing property of ℓ_1 norm mentioned in [117,156].

With a quadratic data term and a ℓ_1 norm regularizer the cost function is of the form

$$C(x) = \| Ax - b \|^2_2 + \| x \|_1. \quad (2.58)$$

The solution to this lies at the common tangent of the level surface of the ℓ_1 and the ℓ_2 norms [117]. This is because, if the point was not at the common tangent point, by keeping one of the terms fixed it is possible to move along the corresponding level set in a direction which decreases the other term thereby decreasing the cost as a whole as shown in Fig. 2.2a. In Eq. (2.58) the level set corresponding to the ℓ_1 term is a rotated square with corners at the axes and the level set of the quadratic term is a circle for the case of two dimensional data. In this case the chance of the circle intersecting the square is high at the corners rather than the lines especially when the relative size of the circle is high compared to that of the square which can be inferred from Fig. 2.2b.

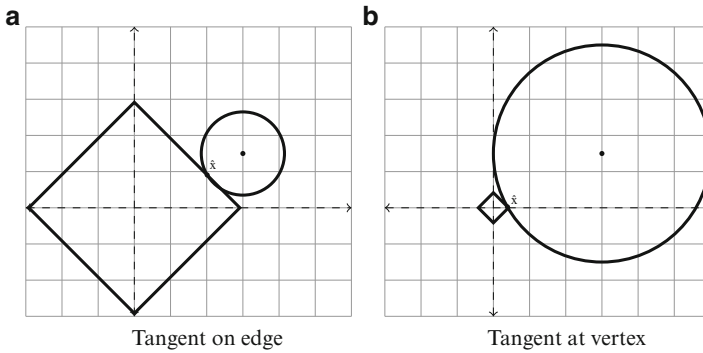


Fig. 2.2 Illustration of sparsity inducing nature of ℓ_1 norm. (a) The solution point is a tangent point of the two level sets (of ℓ_1 and ℓ_2 norms). (b) As the size of the ℓ_2 term increases relative to the ℓ_1 term, the tangent point tends to be the corner of the ℓ_1 level set

Since an image is sparse only in the transform domain or the derivative domain, sparsity is used as a regularizer for estimation in these domains. In Chap. 7 we look at the blind deconvolution problem using sparsity inducing regularizers in the derivative domain and in the wavelet domain. Using ℓ_1 or a variant of it as the regularization term leads to a cost function which is the sum of a differentiable data term and a non-smooth regularizer term. Since the cost function is non-differentiable in this case gradient descent methods will not work. One method of arriving at the optimum of such cost functions is the iterative shrinkage thresholding algorithm (ISTA) which is explained in the next section.

2.6 Optimization Techniques

In this section we look at two of the approaches we use in the monograph for arriving at an optimal solution. One is the alternate minimization technique and the other is iterative shrinkage thresholding algorithm.

2.6.1 Alternate Minimization

As seen in Sect. 2.3.4, blind deconvolution is a bilinear ill-posed problem. Since both the image and the PSF are unknowns, regularizers are used for both. Using square of ℓ_2 norm of the error ($\underline{y} - K\underline{x}$) as the data term the cost function becomes:

$$C(\underline{x}, \underline{k}) = \|\underline{y} - K\underline{x}\|^2 + \lambda_x R_x(x) + \lambda_k R_k(k), \quad (2.59)$$

where λ_x and λ_k are image and PSF regularization factors, and $R_x(x)$ and $R_k(k)$ are the respective regularizers. Since the problem is bilinear in nature, keeping one of the variables fixed makes the data term a quadratic function. If the functions $R_x(x)$ and $R_k(k)$ are chosen to be quadratic functions, keeping one of the variables fixed makes the whole cost quadratic. This makes alternate minimization a natural choice for minimizing the cost given in Eq. (2.59). In addition, keeping one of the variables constant and minimizing w.r.t. the other variable makes the problem a linear ill-posed one at each iteration. The alternate minimization algorithm proceeds as follows:

1. Start with an initial value of $\underline{k}^0 = \underline{k}_{initial}$ and $\underline{x}^0 = \underline{y}$.
2. At the i th iteration, keep \underline{k} fixed at $\underline{k} = \hat{\underline{k}}^{i-1}$ and minimize Eq. (2.59) to obtain a new estimate of \underline{x} , $\hat{\underline{x}}^i$. Here the initial value of \underline{x} is $\hat{\underline{x}}^{i-1}$.
3. Keep \underline{x} fixed at $\hat{\underline{x}}^i$ and minimize the cost to obtain \underline{k} update as $\hat{\underline{k}}^i$, with initial condition on \underline{k} as $\hat{\underline{k}}^{i-1}$.
4. Repeat steps 2 and 3, till some stopping criterion is reached.

The initial value of \underline{k} , $\underline{k}_{initial}$, is chosen as the 2D-discrete impulse. In this monograph we use alternate minimization for solving the blind deconvolution problem. At each step of the alternate minimization method, depending on the cost function obtained, a gradient based method is used to arrive at the optimal points of each step. The AM algorithm generates a sequence of image and PSF pair – $\{(\hat{\underline{x}}^i, \hat{\underline{k}}^i)\}$. We shall study the convergence of this sequence for the TV regularizer and the smoothness based regularizer in subsequent chapters.

2.6.2 Iterative Shrinkage/Thresholding Algorithm

We observed in the previous section that sparsity based solutions use ℓ_1 norm or its variants as a regularizer. With ℓ_1 norm as the regularizer, the cost function becomes the sum of a quadratic data term and a non-differentiable term coming from the regularizer. The usage of ℓ_1 norm calls for optimization methods which can handle

non-differentiable functions. Optimization of such cost functions, for function of a single variable is given below. Let the general form of the cost function be

$$C(x) = f(x) + g(x), \quad (2.60)$$

where both $f(x)$ and $g(x)$ are convex functions with $f(x)$ being a smooth quadratic data term and $g(x)$ a non-smooth regularizer. For solving problems of the type in Eq. (2.60), Moreau's [8, 100] proximal map can be used. Given a closed convex function $h(x)$, the proximal map associated with $h(x)$ is

$$\text{prox}_t(h)(x) := \arg \min_u \left\{ h(u) + \frac{1}{2t} \|u - x\|^2 \right\}, \quad (2.61)$$

where t is a positive constant. Since $g(x)$ in Eq. (2.60) is non-smooth, one can use the subdifferentials [134] to obtain a minimizer. A vector x^* is a minimizer of Eq. (2.60) iff

$$\begin{aligned} 0 &\in t \nabla f(x^*) + t \partial g(x^*), \\ 0 &\in t \nabla f(x^*) + x^* - x^* + t \partial g(x^*), \\ (I + t \partial g)x^* &\in (I - t \nabla f)x^*, \\ x^* &\in (I + t \partial g)^{-1}(I - t \nabla f)x^*. \end{aligned} \quad (2.62)$$

In this set of equations $\partial g(x)$ is the subdifferential of the closed convex non-smooth function $g(x)$. From the last step of Eq. (2.62), an iteration to obtain x^* can be written as

$$x^i = (I + t^i \partial g)^{-1}(I - t^i \nabla f)x^{i-1}. \quad (2.63)$$

It can be shown that [8]

$$(I + t^i \partial g)^{-1}(x) = \text{prox}_{t^i}(g)(x). \quad (2.64)$$

Using Eq. (2.64) in Eq. (2.63) and using the definition of proximal map given in Eq. (2.61),

$$\begin{aligned} x^i &= \text{prox}_{t^i}(g)(x^i - t^i \nabla f(x^{i-1})), \\ &= \arg \min_x \left\{ g(x) + \frac{1}{2t^i} \|x - (x^{i-1} - t^i \nabla f(x^{i-1}))\|^2 \right\}. \end{aligned} \quad (2.65)$$

When $g(x) = \|x\|_1$, the ℓ_1 norm of x , Eq. (2.65) reduces to [8, 99]:

$$x^i = \mathcal{T}_{t^i}(x^{i-1} - t^i \nabla f(x^{i-1})), \quad (2.66)$$

where \mathcal{T}_i is the shrinkage operator defined as

$$\mathcal{T}_\alpha(x^i) = (|x^i| - \alpha)_+ \text{sgn}(x^i), \quad (2.67)$$

where $(a)_+ = \max(a, 0)$ and $\text{sgn}(x)$ is the signum function. When $f(x)$ is the quadratic data term in Eq. (2.59) (with K constant), Eq. (2.66) becomes the iterative shrinkage threshold algorithm (ISTA) [29].

Blind Image Deconvolution

Methods and Convergence

Chaudhuri, S.; Velmurugan, R.; Rameshan, R.

2014, XV, 151 p. 33 illus., 16 illus. in color., Hardcover

ISBN: 978-3-319-10484-3